Available online at www.sciencedirect.com

ScienceDirect

Ceramics International 40 (2014) 2115–2120

CERAMICS INTERNATIONAL

www.elsevier.com/locate/ceramint

Facile synthesis of CoAl-LDH/MnO_2 hierarchical nanocomposites for high-performance supercapacitors

Zeng Peng Diao[a], Yu Xin Zhang[a,b,*], Xiao Dong Hao[a], Zhong Quan Wen[b]

[a]College of Materials Science and Engineering, Chongqing University, Chongqing 400044, P.R. China
[b]Key Laboratory of Fundamental Science of Micro/Nano-Devices and System Technology, Chongqing University, Chongqing 400044, P.R. China

Received 24 June 2013; received in revised form 25 July 2013; accepted 26 July 2013
Available online 3 August 2013

Abstract

In this work, MnO_2/CoAl-layered double hydroxide (CoAl-LDH) nanocomposites were prepared through a simple redox reaction between Co^{2+} species and MnO_4^-. The structure and morphology of these nanocomposites were investigated by powder X-ray diffraction (XRD), Fourier transform infrared spectroscopy (FTIR), focused ion beam scanning electron microscopy (FIB/SEM) and high-resolution transmission electron microscopy (HRTEM). CoAl-LDH/MnO_2 nanocomposites presented their platelet-like structures with MnO_2 nanocrystals decorating the LDH host layer. Furthermore, the electrochemical properties of composites were evaluated by cycle voltammetric (CV) and galvanostatic charge–discharge measurements. Surprisingly, the hierarchical CoAl-LDH/MnO_2 composites displayed a high specific capacitance (1088 F g^{-1} at 1 A g^{-1}), high rate capability, and excellent long-term cycling life. In principle, these findings suggested that CoAl LDHs-based nanocomposites could be promising candidates for supercapacitors electrode with enhancive electrochemical behavior.

Keywords: B. Nanocomposites; E. Electrodes; CoAl-LDH; MnO_2; Supercapacitors

1. Introduction

Layered double hydroxides (LDHs), known as anionic clays or hydrotalcite-like compounds, were represented as the general formula $[M^{2+}_{1-x}M^{3+}_x(OH)_2](A^{n-}_{x/n})_3 \cdot mH_2O$, where M^{2+} was a divalent cation (Mg^{2+}, Zn^{2+}, Cu^{2+}, Ni^{2+}, Co^{2+} etc.), M^{3+} was a trivalent cation (Al^{3+}, Fe^{3+}, Cr^{3+} etc.), A^{n-} was an interlayer anion (CO_3^{2-}, SO_4^{2-}, NO_3^-, Cl^-, OH^-, etc.), and x was the ratio of divalent to trivalent cations [1,2]. Due to their flexible ion-exchange ability and tunable composition, they have attracted interests in the application of electrodes materials for supercapacitors [3–8]. Among various LDHs materials, CoAl-LDH was prominent due to its high specific capacitance and various production methods. For example, Zhang et al. fabricated the pure CoAl-LDH electrode with a high specific capacitance of 641 F g^{-1} at the current density of 1 A g^{-1} in 6 M KOH solution [3]. However, they usually suffered from low rate and poor cycling stability at high current density. For instance, Fang et al. reported that the high specific capacitance of CoAl-LDH was 704 F g^{-1} at 1 A g^{-1}, while it decreased to 400 F g^{-1} at 8 A g^{-1} (with only 56.8% retained) [9].

In attempts to improve the electrochemical performance of CoAl-LDHs-based electrodes, CoAl-LDHs nanocomposites have been studied, as well as CoAl-LDHs-carbon composites involving high surface-area conductive materials such as carbon nanotubes [10,11] and graphene nanosheets [9,12,13]. Although these materials can improve the conductivity of the composites and shorten the diffusion pathways of electron and ion with the aim of more efficient charge and mass exchange, their high costs limited their wide application. And thus, several strategies have been proposed, such as incorporating CoAl-LDHs with other metal oxides (e.g., MnO_2). MnO_2, one of pseudocapacitive transition-metal oxides, has been extensively used in electrochemical application due to their high capacitance, low cost and environment-friendliness [14–22]. Very recently, it was reported that the Co_3O_4@MnO_2 hybrid nanowire arrays exhibited a high capacitance with good cycle performance and remarkable rate capability [23]. Moreover, we successfully fabricated MnO_2

*Corresponding author at: College of Materials Science and Engineering, Chongqing University, Chongqing 400044, P.R. China.
Tel./fax: +86 23 65104131.
E-mail address: zhangyuxin@cqu.edu.cn (Y.X. Zhang).

0272-8842/$ - see front matter © 2013 Elsevier Ltd and Techna Group S.r.l. All rights reserved.
http://dx.doi.org/10.1016/j.ceramint.2013.07.127

nanoparticles into various crystallographic types and crystal morphologies of MnO_x nanostructures with a high specific capacitance and excellent rate ability [24]. Taking into consideration of these promising advantages, the combination of CoAl-LDH and MnO_2 may improve the stability of composites electrode at high current density.

Herein, we have developed a facile, inexpensive and template-free method of CoAl-LDH/MnO_2 nanocomposties through a simple redox reaction. The structure and morphology of the nanocomposites were investigated. Moreover, the effects of preparative parameters (e.g., process time and temperature) on enhanced electrochemical performance of CoAl-LDH/MnO_2 nanocomposties were examined.

2. Experimental section

2.1. Synthesis of CoAl-LDH/MnO_2 composites

CoAl-LDH (denoted as CALDH) and CoAl-LDH/MnO_2 nanocomposites (denoted as CALDHM) were obtained by a modified co-precipitated method [25]. In a typical synthesis, $Co(NO_3)_2 \cdot 6H_2O$ (0.01 mol), $Al(NO_3)_3 \cdot 9H_2O$ (0.005 mol), and urea (0.35 mol) were dissolved in deionized water (0.5 L) with $n(Co^{2+}):n(Al^{3+})=2:1$. After 30-min ultra-sonication, the homogeneous solution was subjected to reflux at 98 °C for 48 h under vigorous stirring. Subsequently, CALDH were washed with distilled water for several times, followed by redispersion in $KMnO_4$ (100 mL, 0.05 M) at pre-designated temperatures (e.g., room temperature, 60 °C, and 120 °C). Then the resulting CALDHM products were collected by centrifugation/washing for several times.

In order to clarify these samples, the composites were termed as CALDHM-*t*-*T*, where *t* and *T* stood for deposition time and temperature with $KMnO_4$ solution, respectively. For example, CALDHM-1-RT meant CoAl-LDH/MnO_2 nanocomposites prepared through the reaction of CoAl-LDH in $KMnO_4$ solution for 1 h at room temperature.

2.2. Materials characterization

The crystallographic information and chemical composition of as-prepared products were established by powder X-ray diffraction (XRD, D/max 1200, Cu K_α) and Fourier transform infrared spectroscopy (FTIR, Nicolet 5DXC). The structural and morphological investigations of these samples were carried out by focused ion beam scanning electron microscopy (FIB/SEM, ZEISS AURIGA) and high resolution transmission electron microscopy (HRTEM, ZEISS LIBRA 200).

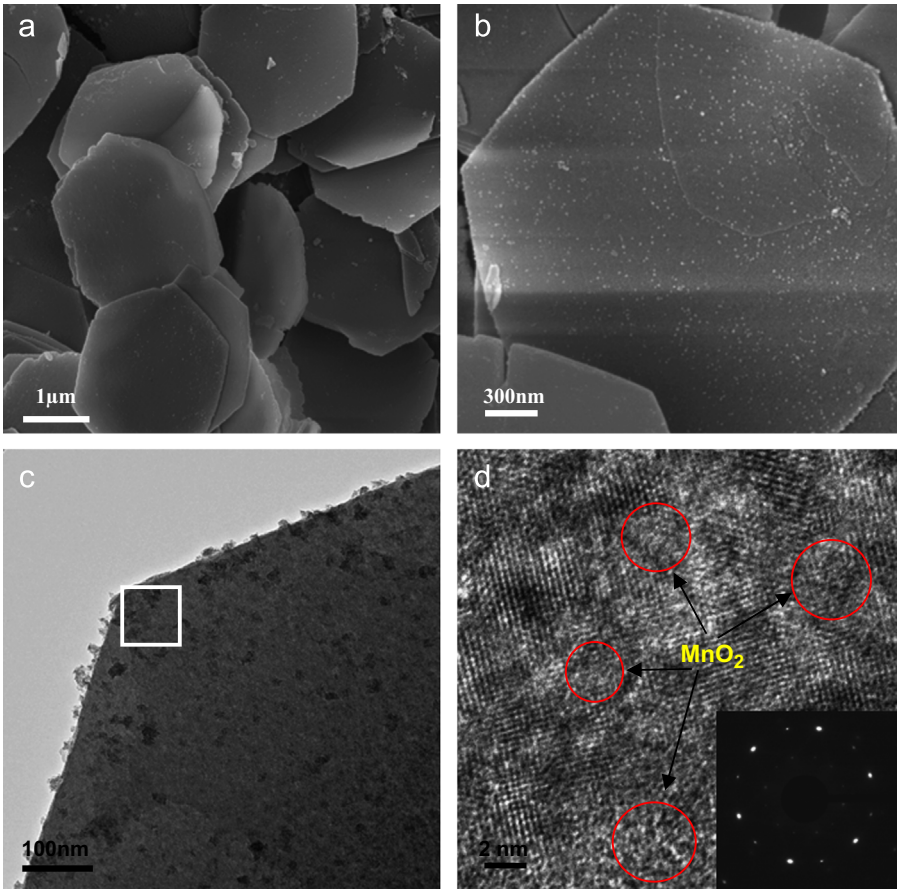

Fig. 1. SEM images of CoAl-LDH (a) and CoAl-LDH/MnO_2 nanocomposites (CALDHM-1-RT) (b). TEM and HRTEM images of CALDHM-1-RT (c, d). The inset: corresponding SAED pattern of the area indicated by the white rectangle in (c). (For interpretation of the references to color in this figure, the reader is referred to the web version of this article.)

2.3. Electrochemical measurement

The electrochemical performance of CALDHM nanocomposites were carried out on the CHI 660E electrochemical workstation in KOH solution (6.0 M). For the tests with a three-electrode configuration, the working electrodes were CALDHM nanocomposites prepared in this work. Platinum plate was used as the counter electrode and saturated Hg/HgO electrode as the reference. Cyclic voltammetry was performed in a potential range between −0.05 and 0.40 V at different scan rates. Galvanostatic charge/discharge curves were obtained by cycling the potential from 0 V to 0.38 V at various current densities to evaluate the specific capacitance. The electrochemical impedance spectroscopy (EIS) measurements were conducted in a frequency range from 100 kHz to 0.01 Hz with perturbation amplitude of 5 mV.

3. Results and discussion

3.1. Structure and morphology

Representative SEM and TEM images of CALDH and CALDHM-1-RT are presented in Fig. 1. As shown in Fig. 1a, the CALDH samples consisted of regular and thin hexagonal platelets with a mean lateral size of ~2.54 μm, indicative of high quality in size and morphology. According to the chemical bonding theory of single crystal growth [26], crystal growth is controlled by both thermodynamic and kinetic factors, crystallographic limitations are a key thermodynamic factor [27], varying conditions are kinetic parameters [28], when we engineer materials morphology via solution routes. The hexagonal morphology of these particles is thus ascribed to the rhombohedral structure of LDH, however, the uniformity and high crystallinity can be attributed to the slow growth rate of LDH upon corresponding slow hydrolysis of urea [25].

As shown in Fig. 1b, the typical CALDHM platelets morphology remained unchanged in initial stage (reaction within 60 min), while MnO_2 nanoparticles were finely dispersed on the hexagonal platelets of CALDH host layer (Fig. 1c,d). Interestingly, the sites of MnO_2 nanocrystals could indirectly reveal the uniform distribution of Co element on the LDH layer, since Zhao et al. verified that redox reaction would spontaneously occur between the Co^{2+} species within LDH and $KMnO_4$ in solution, leading to the generation of MnO_2 nanocrystals [29]. Moreover, the HRTEM images and corresponding selected area electron diffraction (SAED) pattern (inset in Fig. 1d) could also verify high crystallinity of the LDH support; Meanwhile indistinct areas (red circles in Fig. 1d) indicated amorphous MnO_2.

In attempts to further investigate formation of CALDHM, processing time and temperatures were tuned (See Supplementary Information, SI-1). By extending the processing time to 2 h, it can be found that a bit of fragments came out on the LDH host layer, indicating that the structure damage took placed under the excess redox reaction. Moreover, elevated temperature also caused the crush of LDH layer. Thus, it turned out that the optimized preparative conditions of CALDHM ternary nanocomposites should be well controlled under mild conditions.

In order to make clear the MnO_2 formation in CALDHM composites, XRD pattern of as-prepared CALDH and CALDHM is presented in Fig. 2 and Fig. 3 respectively. In Fig. 2, all the diffraction peaks could be indexed as rhombohedral structure of LDH with the refined lattice parameters of $a=0.30726$ nm and $c=2.26032$ nm, in accord with well-known LDH materials in CO_3^{2-} forms [25]. Additionally, the sharp and symmetric features of the diffraction peaks without any other peaks of impurities strongly suggested that the as-prepared CALDH was highly crystallized. After the redox reaction, it can be seen in Fig. 3 that the main strong basal (00*l*) reflection kept constant after reaction at room temperature for 1–2 h, while slight shift occurred on lattice parameter of CALDH. More specifically, Table 1 lists the indexing of XRD patters of CALDHM, compared to that of the pristine

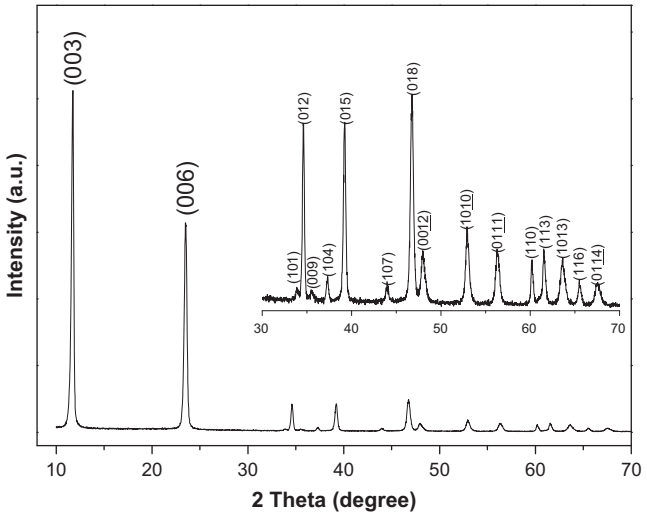

Fig. 2. XRD patterns of as-prepared CoAl-LDH. The Inset: enlarged view of the pattern in high angles.

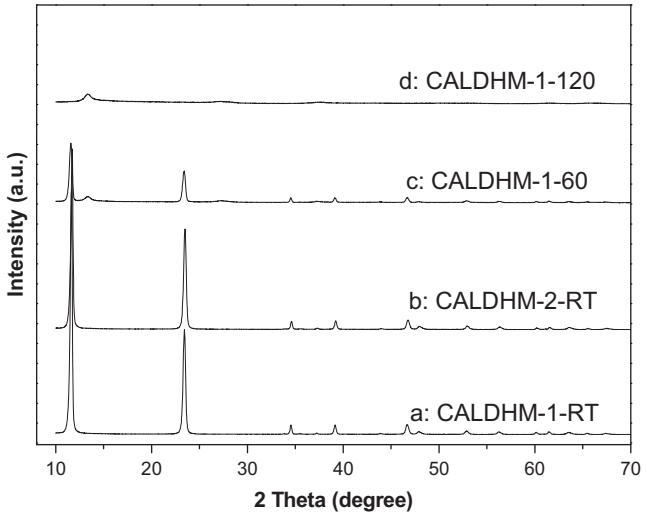

Fig. 3. XRD patterns of CoAl-LDH/MnO_2 nanocomposites prepared with various experimental conditions: deposition in $KMnO_4$ solution (0.05 M) at room temperature for 1 h (a) and 2 h (b), respectively; deposition with $KMnO_4$ solution for 1 h at 60 °C (c) and 120 °C (d), respectively.

Table 1
Indexing of XRD patterns of samples.

Sample	d_{003} (nm)	d_{006} (nm)	d_{009} (nm)	d_{110} (nm)	Crystallite size in *c* direction (nm)	Crystallite size in *a* direction (nm)
CALDH	0.75264	0.37691	0.25126	0.15363	2.26023	0.30726
CALDHM-1-RT	0.75917	0.37912	0.25239	0.15379	2.27458	0.30758
CALDHM-2-RT	0.75418	0.37849	0.25222	0.15356	2.26782	0.30712

Note: *c* was the average value of $3d_{003}$, $6d_{006}$, $9d_{009}$; $a=2\ d_{110}$.

CALDH. The calculated crystallite sizes in *c* direction of CALDH-1-RT and CALDH-2-RT were 2.27458 and 2.26782 nm, respectively. Moreover, by elevating the reaction temperature to 60 °C and 120 °C, the basal reflection of LDH declined, indicating the crush and damage of the layer structure of the samples, corresponding to the results (SI-1).

Fig. 4 depicts the FTIR spectra of CALDH and CALDHM nanocomposites. As can be seen, the broad adsorption band at 3458 cm^{-1} was attributed to O–H stretching modes of interlayer water molecules and H-bonded OH groups, and the corresponding bending mode of water molecules appeared at about 1633 cm^{-1}. The strong peaks at 1358 and 762 cm^{-1} belonged to ν_3 vibration and bending modes of CO_3^{2-}, respectively [25]. The weak absorbance bands in the range of 800–400 cm^{-1} were due to the lattice vibration bands of the M–O and O–M–O (where M=Co, Al) groups, in good agreement with literatures [30]. Compared to pristine CALDH, there was no apparent change on the FTIR spectra of CALDHM after one-hour reaction, indicating that the mild reaction occurred among the LDH host layer and permanganate group. By elevating the reaction temperature to 60 °C and 120 °C, the intensity of absorption peak at 1358 cm^{-1} decreased, possibly caused by the decomposition of carbonate group within the intense reaction. And a sharp absorption peak at 573 cm^{-1} emerged, indicative of the substantial generation of MnO_2 phase.

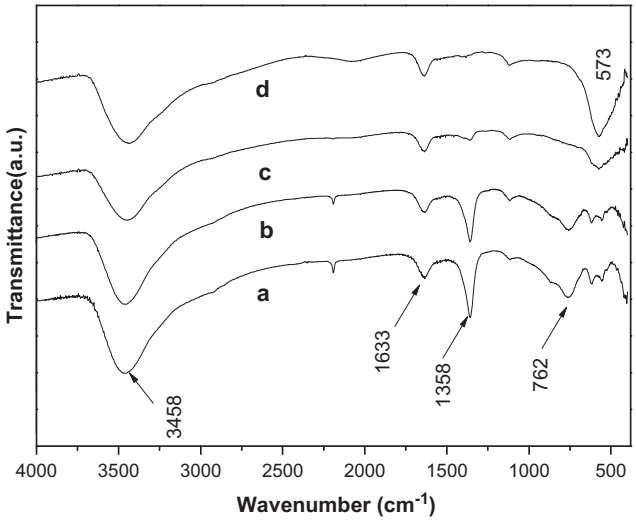

Fig. 4. FTIR spectra of CoAl-DH (a), and CoAl-LDH/MnO_2 nanocomposites obtained by at different temperature: (b) room temperature, (c) 60 °C and (d) 120 °C. Experimental conditions: dispersion LDH in $KMnO_4$ solution (0.05 M) for 1 h.

3.2. Electrochemical behavior

CV curves of CALDHM-1-RT are presented in Fig. 5a. The quasi-rectangular CV curves were attributed to the reversible intercalation/de-intercalation processes among the electrolyte. As the scan rate was 5 mV s^{-1}, there was one well-defined peak at 219 mV, belonging to the conversion of Co(II)/Co(III) [11]. With the increase of scan rate, the anodic and cathodic peaks moved towards positive and negative direction, respectively.

Fig. 5b shows the galvanostatic charge–discharge curves of CALDHM-1-RT. The specific capacitance (Cs) can be obtained from discharge curves according to the following equation:

$$C_s = \frac{I\Delta t}{m\Delta V} \quad (1)$$

where *I*, Δt, ΔV, and *m* are the constant current (A), discharge time (s), total potential deviation (V), and mass of active materials (g), respectively [12]. The specific capacitance of CALDHM-1-RT was 1088 F g^{-1} at the current density of 1 A g^{-1}, larger than those of other CoAl-LDH-based nanocomposties [9,12]. It was found that ca. 67% of the capacitance was still retained as the discharge current density increased to 10 A g^{-1}, higher than those of MnO_2-based electrodes and hybrid pseudo-capacitive materials [31,32]. Notably, even at a high current density of 20 A g^{-1}, the retention percentage of capacitance reached 50.3%, indicating its great rate capability.

Fig. 5c displays the CVs of CALDHM-1-RT, CALDHM-1-60 and CALDHM-1-120 nanocomposites at the scan rates of 20 mV s^{-1}. Clearly, the area of the closed quasi-rectangular CV curves (CALDHM-1-60 and CALDHM-1-120) decreased drastically, compared to that of CALDHM-1-RT. This result could be caused by the crush of LDH support, as discussed above. In order to further address the effect of the preparative parameters on the capacitor performance on the CoAl-LDH/MnO_2 system, the galvanostatic charge-discharge curves for the CALDH and CALDHM nanocomposites at a current density of 1 A g^{-1} are revealed in Fig. 5d. Symmetric charge–discharge curves indicated its higher coulombic efficiency and super electrochemical reversibility. Yet, compared to that of CALDHM-1-RT, the capacitive value of CALDH and CALDH-2-RT were 876 F g^{-1} and 785 F g^{-1} respectively, indicative of a slightly reduction. These findings indicated that a proper amount of MnO_2 anchored on the LDH support would enhance the supercapacitor performance, in coincidence with the previous work [29]. Moreover, the influence of the current density on the capacitance is disclosed in SI-2. It was also found that CALDHM-1-RT evinced the

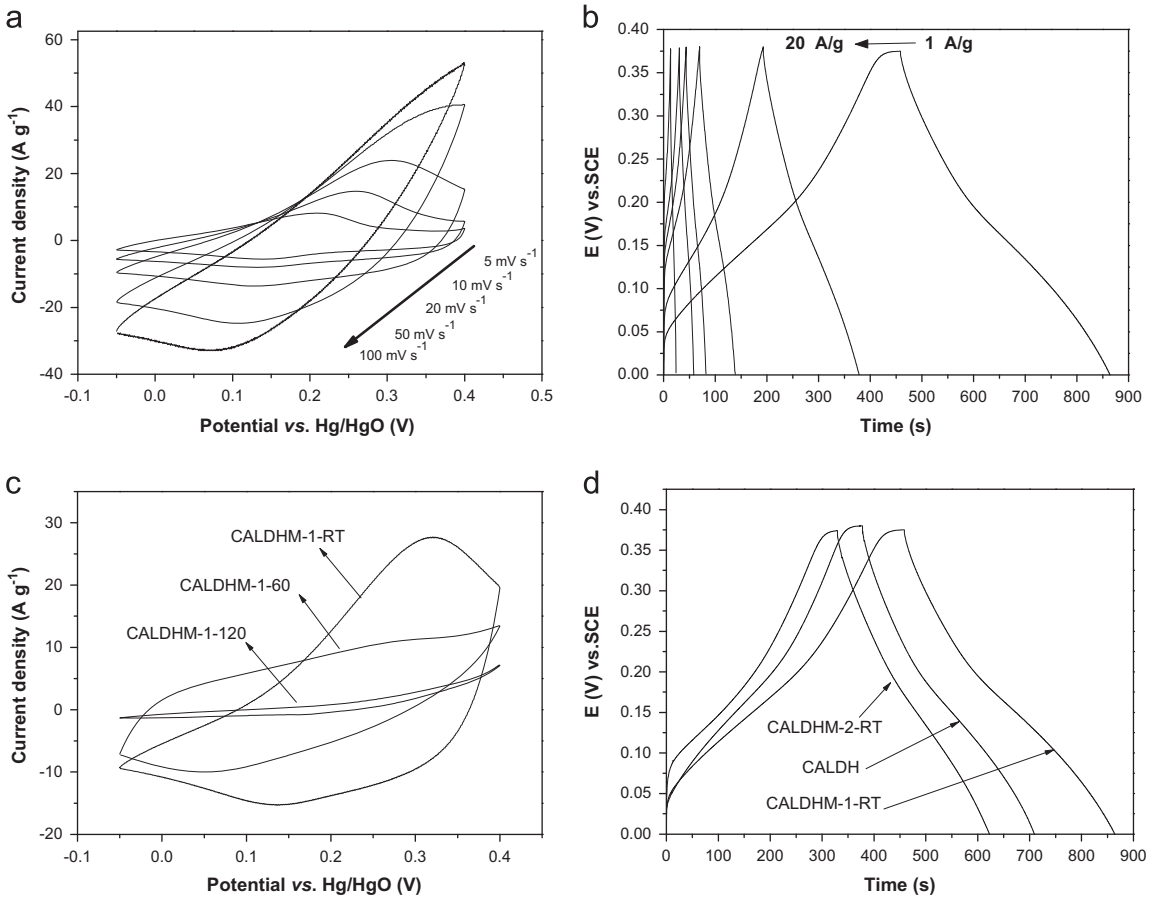

Fig. 5. CVs and galvanostatic charge–discharge curves of CoAl-LDH/MnO_2 nanocomposites (a, b) (CALDHM-1-RT) at various test conditions (the discharge current densities: from 1 A g^{-1} to 2, 5, 8, 10, 20 A g^{-1}); CVs of CoAl-LDH/MnO_2 nanocomposites at scan rates of 20 mV s^{-1}, (c) experimental conditions: deposition in $KMnO_4$ solution at elevated temperature (RT, 60 °C, 120 °C) for 1 h; Galvanostatic charge–discharge curves and (d) for the CoAl-LDH and CoAl-LDH/MnO_2 nanocomposites at a current density of 1 A g^{-1}. Experimental conditions: deposition in $KMnO_4$ solution at room temperature for 1–2 h.

greatest current rates stability; meanwhile the other two samples had small deduction of capacitance.

The electrochemical impedance spectroscopy (EIS) of CALDH-1-RT and CALDH-2-RT nanocomposites in 6 M KOH solution are depicted in Fig. 6. At very high frequencies, the intercept at real part (Z′) was a combinational resistance of ionic resistance of electrolyte, intrinsic resistance of substrate and contact resistance at the active materials/current collector interface. In the low-frequency range, a semicircle could be found, whose diameter stood for the charge transfer resistance, caused by the Faradic reaction and the double-layer capacitance on the grain surface. The results indicated that CALDHM-1-RT showed better electronic transport and lower charge transfer resistance than that of CALDHM-2-RT.

Cycling capability is an important requirement for supercapacitor applications. Fig. 7 displays the cycling life tests for CALDHM-1-RT. No obvious decrease of specific capacitance after 1000 cycles was observed in the galvanostatic charge and discharge curve, which reflected the stability of the electrochemical performance. This finding was further verified by the stable charge-discharge curves for the last 15 cycles (Fig. 7). Hence, it can be concluded that the rational combination of MnO_2 and LDH into an integrated architecture could substantially improve the electrochemical properties.

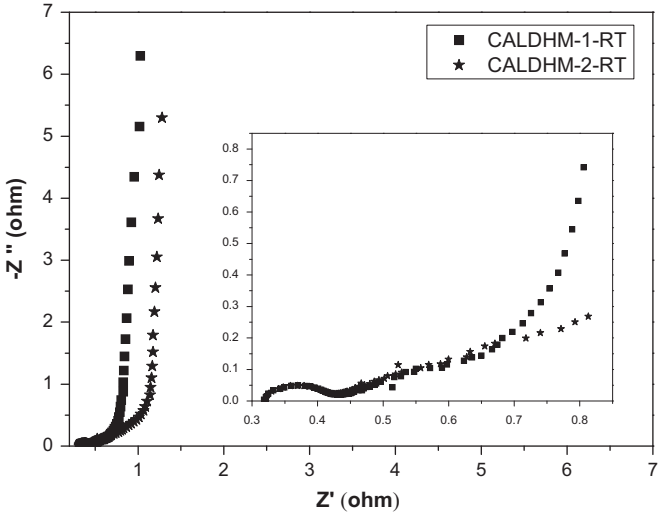

Fig. 6. Nyquist plots of the CoAl-LDH/MnO_2 nanocomposites. Experimental conditions: deposition in $KMnO_4$ solution at room temperature for 1 h (CALDHM-1-RT); 2 h (CALHDM-2-RT), respectively.

4. Conclusion

In summary, CoAl-LDH/MnO_2 nanocomposites with regular and thin hexagonal platelet were successfully prepared by a facile

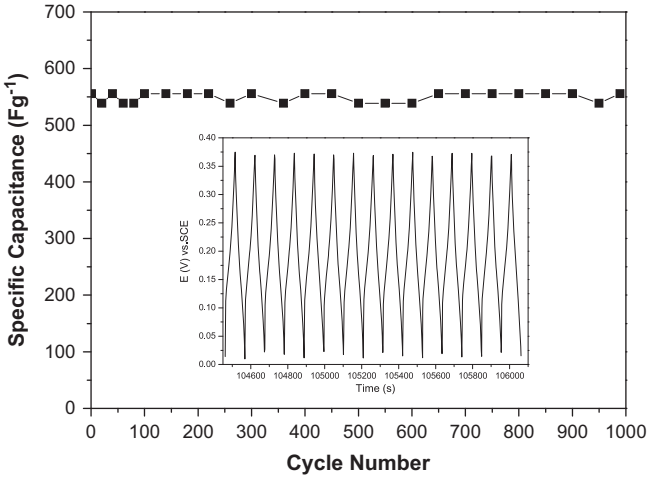

Fig. 7. Cycling performance of CoAl-LDH/MnO_2 nanocomposites (CALDHM-1-RT) at current density of 6 A g^{-1}. The inset: the charge–discharge curves of the last 15 cycles.

route. By fine-tuning the preparative parameters (e.g., reaction time and temperature), uniform nanocomposites can be well-controlled under the mild reaction (e.g., 1 h at room temperature) between CoAl-LDH and $KMnO_4$ solution. Owing to the synergistic effect of the active materials and the unique hierarchical structure, the resulting CoAl-LDH/MnO_2 nanocomposites electrode exhibited a large specific capacitance, good rate capability and excellent long-term cycle stability. In principles, this synthetic approach could be extended for the fabrication of other LDHs-based nanocomposites for promising electrode candidates in energy storage devices.

Acknowledgment

The authors gratefully acknowledge the financial supports provided by the National Natural Science Foundation of China (Grant no. 51104194), the Doctoral Fund of Ministry of Education of China (20110191120014), No. 43 Scientific Research Foundation for the Returned Overseas Chinese Scholars, State Education Ministry and Fundamental Research Funds for the Central Universities (Project nos. CDJZR12248801 and CDJZR12135501, Chongqing University, PR China). Dr. Zhang would also like to thank Chongqing University for providing Talent of High Level Scientific Research Fund.

Appendix A. Supporting information

Supplementary data associated with this article can be found in the online version at http://dx.doi.org/10.1016/j.ceramint.2013.07.127.

References

[1] F. Cavani, F. Trifirò, A. Vaccari, Catalysis Today 11 (1991) 173–301.
[2] X. Duan, D.G. Evans, Layered Double Hydroxides, Springer, Verlag, Berlin Heidelberg, 2006.
[3] L. Zhang, X. Zhang, L. Shen, B. Gao, L. Hao, X. Lu, F. Zhang, B. Ding, C. Yuan, Journal of Power Sources 199 (2012) 395–401.
[4] L. Wang, D. Wang, X.Y. Dong, Z.J. Zhang, X.F. Pei, X.J. Chen, B. Chen, J. Jin, Chemical Communications 47 (2011) 3556–3558.
[5] J. Jiang, J. Zhu, R. Ding, Y. Li, F. Wu, J. Liu, X. Huang, Journal of Materials Chemistry 21 (2011) 15969–15974.
[6] M. Shao, F. Ning, Y. Zhao, J. Zhao, M. Wei, D.G. Evans, X. Duan, Chemistry of Materials 24 (2012) 1192–1197.
[7] Y. Liu, R. Li, Z. Li, Y. Fang, J. Liu, Electrochimica Acta 94 (2012) 360–366.
[8] C. Mousty, F. Leroux, Recent Patents on Nanotechnology 6 (2012) 174–192.
[9] J. Fang, M. Li, Q. Li, W. Zhang, Q. Shou, F. Liu, X. Zhang, J. Cheng, Electrochimica Acta 85 (2012) 248–255.
[10] L.H. Su, X.G. Zhang, Y. Liu, Journal of Solid State Electrochemistry 12 (2007) 1129–1134.
[11] L. Su, X. Zhang, C. Yuan, B. Gao, Journal of the Electrochemical Society 155 (2008) A110–A114.
[12] S. Huang, G.N. Zhu, C. Zhang, W.W. Tjiu, Y.Y. Xia, T. Liu, ACS Applied Materials and Interfaces 4 (2012) 2242–2249.
[13] W. Zhang, C. Ma, J. Fang, J. Cheng, X. Zhang, S. Dong, L. Zhang, RSC Advances 3 (2013) 2483–2490.
[14] K. Chen, Y. Dong Noh, K. Li, S. Komarneni, D. Xue, Journal of Physical Chemistry C 117 (2013) 10770–10779.
[15] Y. Zhang, C. Sun, P. Lu, K. Li, S. Song, D. Xue, Crystal Engineering Communications 14 (2012) 5892–5897.
[16] G. Yu, L. Hu, M. Vosgueritchian, H. Wang, X. Xie, J.R. McDonough, X. Cui, Y. Cui, Z. Bao, Nano Letters 11 (2011) 2905–2911.
[17] Z. Li, Y. Mi, X. Liu, S. Liu, S. Yang, J. Wang, Journal of Materials Chemistry 21 (2011) 14706–14711.
[18] X. Li, B. Wei, Nano Energy 1 (2012) 479–487.
[19] P. Li, Y. Song, Z. Tang, G. Yang, Q. Guo, L. Liu, J. Yang, Ceramics International 39 (2013) 7773–7778.
[20] P. Yang, X. Xiao, Y. Li, Y. Ding, P. Qiang, X. Tan, W. Mai, Z. Lin, W. Wu, T. Li, ACS Nano 7 (2013) 2617–2626.
[21] C. Chen, H. Chang, S. Shih, C. Tsay, C. Chang, C. Lin, Ceramics International 39 (2013) 1885–1892.
[22] L. Mai, F. Dong, X. Xu, Y. Luo, Q. An, Y. Zhao, J. Pan, J. Yang, Nano Letters 13 (2013) 740–745.
[23] J. Liu, J. Jiang, C. Cheng, H. Li, J. Zhang, H. Gong, H.J. Fan, Advanced Materials 23 (2011) 2076–2081.
[24] Y.X. Zhang, S.J. Zhu, M. Dong, C.P. Liu, Z.Q. Wen, International Journal of Electrochemical Science 8 (2013) 2407–2416.
[25] Z. Liu, R. Ma, M. Osada, N. Iyi, Y. Ebina, K. Takada, T. Sasaki, Journal of the American Chemical Society 128 (2006) 4872–4880.
[26] X. Yan, D. Xu, D. Xue, Acta Materialia 55 (2007) 5747–5757.
[27] C. Sun, D. Xue, Journal of Physical Chemistry C 117 (2013) 5505–5511.
[28] D. Xue, X. Yan, L. Wang, Powder Technology 191 (2009) 98–106.
[29] J. Zhao, Z. Lu, M. Shao, D. Yan, M. Wei, D.G. Evans, X. Duan, RSC Advances 3 (2013) 1045–1049.
[30] H. Peng, Y. Han, T. Liu, W.C. Tjiu, C. He, Thermochimica Acta 502 (2010) 1–7.
[31] R.R. Salunkhe, K. Jang, S. Lee, H. Ahn, RSC Advances 2 (2012) 3190–3193.
[32] X. Lu, T. Zhai, X. Zhang, Y. Shen, L. Yuan, B. Hu, L. Gong, J. Chen, Y. Gao, J. Zhou, Advanced Materials 24 (2012) 938–944.